ELSEVIER

Mechatronics 14 (2004) 255–280

MECHATRONICS

Non-dimensionalized performance indices based optimal grasping for multi-fingered hands

Byoung-Ho Kim [a,b], Byung-Ju Yi [a,*], Sang-Rok Oh [b], Il Hong Suh [a]

[a] *School of Electrical Engineering and Computer Science, Hanyang University, 1271 Sa 1-dong, Ansan, Kyungki 425-791, South Korea*

[b] *Intelligent System Control Research Center, KIST, Seoul 136-791, South Korea*

Abstract

When a multi-fingered hand grasps an object, the ways to grasp it stably are infinite, and thus an optimal grasp planning is necessary to find the relatively optimized grasp points on object for achieving the objective of the given grasping and manipulating task. For this, we first define several grasp indices to evaluate the quality of each feasible grasp. Since the physical meanings of the defined grasp indices are different from each other, it is not easy to combine those indices to identify the optimal grasping. Thus, we propose a new generalized grasping performance index to represent all of the grasp indices as one measure based on a non-dimensionalizing technique. Next, by using the proposed grasping performance index, we try to determine the optimal grasp points for multi-fingered hands performing contact tasks. Through task-based simulation studies, we discuss the feasibility of each grasp index as the grasp polygons and then, we show that the trend of the proposed optimal grasp planning is coincident to the physical sense of human grasping. Furthermore, some experimental results showing the task specific performances are incorporated to corroborate the effectiveness of the proposed optimal grasp planning algorithms.

Keywords: Multi-fingered hands; Optimal grasp planning; Generalized grasping performance index

1. Introduction

When a multi-fingered hand grasps an object, the ways to grasp it stably are infinite and thus an optimal grasp planning is required to find the optimal grasp points

* Corresponding author. Fax: +82-345-416-6416.
E-mail address: bj@hanyang.ac.kr (B.-J. Yi).

0957-4158/$ - see front matter
doi:10.1016/S0957-4158(03)00039-4

to satisfy the objective of the given task. In determination of grasp points on object, it is very important to select grasp points in such a way to minimize the grasp error caused by external uncertainties. Even though the selected grasp points are stable, the most stable grasp points are necessary for dextrous manipulation of object.

Many research works have focused on the field of manipulating object grasped by multi-fingered hands [1–6]. For dextrous manipulation of object, it is necessary to grasp the most stable points on object. Some researchers tried to find the proper grasp points using some grasp indices [7–11]. Li and Sastry [7] defined a grasp index that is made up of the singular value of a grasp matrix, the volume of wrench space, and the task ellipsoid. They focused on finding optimal grasp points by optimization of the defined grasp index. In this method, the required maximum forces for all directions of each fingertip not only must be known, but also the procedure of computing the defined grasp index is rather complex. Cutkosky [8] defined various analytical grasp indices for grasp modeling and effective selection of grasp points, and also classified systematic grasp styles considering the grasp geometry and the task characteristics of the given task. Through Cutkosky's work, it is known that grasp configuration and manipulability of multi-fingered hands may be different depending upon the grasp style. Therefore, we can notice that grasp points should be carefully chosen by considering the objective of the given task. Park and Starr [9] proposed two different grasp indices such as uncertainty grasp index and task compatibility grasp index reflecting force and velocity transmission ratios. However, since this method is based on hybrid position and force control, the task space must be classified in advance. Thus, the method can be applied to limited cases. In [10], three-fingered grasp synthesis has been studied for polygonal objects in two-dimensional space. Here, feasible grasp combinations are sorted as the contact models and a force closure grasp based on the object geometry is constructed. Also, grasp search using heuristic function is employed to find the optimal grasp points. In this process of searching the optimal grasp points, the normal directional contact between finger and object is only treated and the heuristic function is dependent upon the limited geometrical condition. So, extension of this method to three-dimensional space is not easy and also the manipulable grasp characteristic is not considered yet. In [11,12], optimal grasp point based on the self-posture changeability of each finger was reported. Using Kaneko's work [11], contact point detection for grasping can be achieved even though the exact object position and shape are not known a priori. Recently, Lin et al. [13] used a stiffness-based grasp measure for achieving compliant grasp.

In this paper, we propose a method to find the optimal grasp points of the given object with respect to a non-dimensionalized composite grasp index. In Section 2, we first define several grasp indices to evaluate the quality of each feasible grasp. In Section 3, after normalizing each grasp index, we present a non-dimensionalized composite grasp index that combines all of the grasp indices as one measure. In order to validate the effectiveness of the proposed optimal grasping approach, task-based simulation studies are presented in Section 4. In Section 5, some experimental results will be shown to corroborate the effectiveness of the proposed optimal grasp planning algorithms. Finally, we draw concluding remarks in Section 6.

2. Grasp indices

For stable grasping and manipulation of an object, it is very important to select the stable grasp points and then proper hand/arm coordination may be required to guarantee stable manipulation for the given trajectory [1–3]. Therefore, in the manipulating tasks using multi-fingered hands, an optimal grasping strategy is necessary to find the optimal grasp points. Also, optimal grasping problem is usually associated with the control objective of the given task, the geometry of object, and the structure of hand [8]. Thus, to determine the optimal grasp points of fingers, it is desirable to take into account task constraints, object constraints, and hand constraints as shown in Fig. 1, simultaneously.

Here, we define several grasp indices to evaluate the quality of given grasps:

- stability grasp index, I_S,
- uncertainty grasp index, I_U,
- maximum force transmission ratio index, $\bar{\sigma}_{F,max}$,
- task isotropy index, σ_{TI},
- stiffness mapping-based grasp isotropy index, σ_{SI}.

2.1. Stability grasp index

The stability grasp index is defined as the quantitative index to evaluate the capability of withstanding external force. For example, consider an L-type object grasped by a three-fingered hand shown in Fig. 2.

In Fig. 2, there exists three types of grasp points as shown in Fig. 3. In case that a finger grasps the convex vertex of the object like Fig. 3(b), the finger may become easily unstable by small external disturbance.

When a finger has to grasp the concave vertex of Fig. 3(c), the manipulable range of the finger must be limited. Thus, we can notice that those points are not adequate as stable and dextrous grasp points. For example, when a three-fingered hand grasps

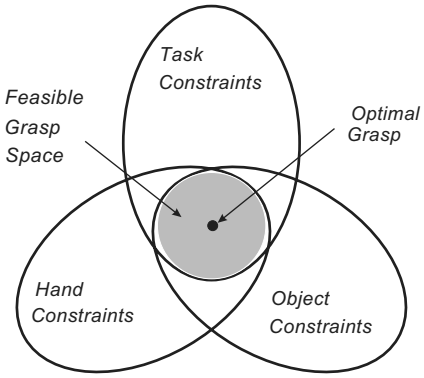

Fig. 1. Optimal grasp of multi-fingered hand.

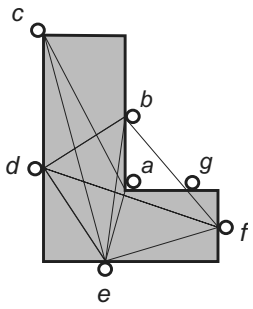

Fig. 2. Grasp points for L-type object.

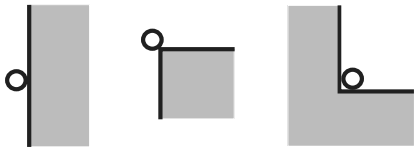

Fig. 3. Types of grasp points: (a) edge, (b) convex vertex, (c) concave vertex.

an object shown in Fig. 2, we can say that the grasp polygon of *bde* is more proper than that of *ace* in aspect of stability. In this sense, we exclude those points among the candidates of optimal grasp points in advance. Practically, it is possible to exclude those points via visual signal processing.

When a multi-fingered hand grasps an object, the grasp region of each finger on object can be classified as the feasible contact region (FCR) and the feasible grasp region (FGR). FCR means the kinematically reachable contact region and FGR implies the grasp region considering friction cone. Those FGR regions can be identified by combining visual signal processing [4,18,19] and tactile signal processing of fingertips [5,6,20].

Then, let us consider Fig. 4 that shows the grasp triangles drawn by connecting the three contact points. The more a grasp triangle forms a regular triangle structure, the more it becomes the form closure grasp [10]. Therefore, we can notice that the desired grasp points should be selected to form a regular polygon structure for stable grasp. In this viewpoint, we define the stability grasp index, I_S, as follows:

$$I_S = \frac{1}{\theta_{\max}} \sum_{i=1}^{n_f} |\theta_i - \bar{\theta}|, \tag{1}$$

where n_f denotes the number of fingers, θ_i is the inner angle for the ith grasp point of the grasp polygon formed by the grasp points, $\bar{\theta}$ given by

$$\bar{\theta} = \frac{180(n_f - 2)}{n_f}$$

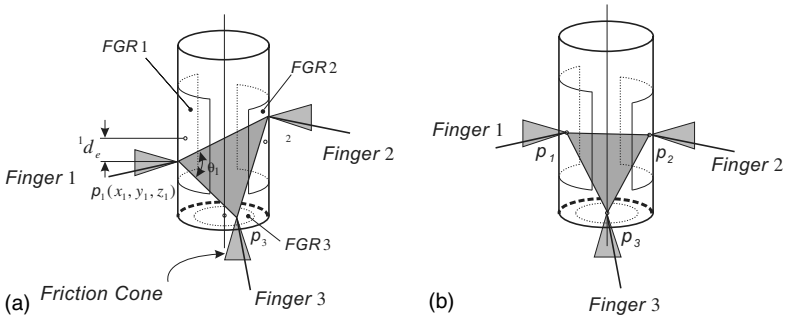

Fig. 4. Grasp triangle as grasp location: (a) any point in FGR, (b) center point in FGR.

denotes the average inner angle of the grasp polygon, and $\theta_{\max}$ defined as

$$\theta_{\max} = \sum_{i=1}^{n_f} |\theta_i - \bar{\theta}|_{\text{ill-conditioned}} = (n_f - 2)(180 - \bar{\theta}) + 2\bar{\theta}$$

implies the case that the grasp polygon has the most ill-conditioned shape such as a line.

From (1), it is pointed out that the stability grasp index is minimized when a grasp polygon has a regular polygon structure.

On the other hand, note that since the defined stability grasp index only considers the shape of achievable grasp polygons, there exists many polygons of same kind. Thus, another grasp index should be incorporated to find the optimal grasp point for each finger.

2.2. Uncertainty grasp index

Even though the grasps formed by the polygons *bde*, *bdf*, and *def* in Fig. 2 are comparably stable, it is not easy to choose the most preferable grasp. In this case, we can determine the relatively better grasp by estimating the position sensitivity as the location of each grasp point changes. Usually, the more a grasp has many grasp points near the edge, the more it may be unstable. In the viewpoint of uncertainty, it is natural that the grasp of Fig. 4(b) is a better grasp comparing to the case of Fig. 4(a). Thus, in order to estimate the position sensitivity of the employed grasp points, we define the uncertainty grasp index as

$$I_U = \frac{1}{n_f} \sum_{i=1}^{n_f} {}^i d_e, \tag{2}$$

where

$${}^i d_e = \sqrt{(x_i - x_{io})^2 + (y_i - y_{io})^2 + (z_i - z_{io})^2},$$

and the position parameters x_i, y_i, and z_i denote the x-, y-, and z-directional position for the grasp point of the ith finger, respectively. And x_{io}, y_{io}, and z_{io} denote the center position of the FGR for the ith finger, respectively.

Consequently, the uncertainty grasp index is minimized when all fingers grasp the center of each feasible grasp region. Since the defined stability and uncertainty grasp indices are dependent on the shape of the given object, those indices can be considered as the performance measures reflecting the object constraints. Particularly, those are useful for estimating the quality of the static grasp.

2.3. Maximum force transmission ratio index

When an object grasped by multi-fingered hands is being manipulated, the force transmission capability of the hand is associated with the grasp geometry of the hand and the configuration of each finger. Thus, it can be considered as a grasp performance measure reflecting the hand and/or object constraints for effective manipulation of an object. For effective manipulation of a grasped object by multi-fingered hands, it is reasonable to select the grasp point of each finger in such a way to minimize the fingertip force.

Consider a peg-in-hole task performed by a n_f-fingered hand given in Fig. 5. The generalized force relation between the operational space $\boldsymbol{O}_o$ and the fingertip space is given by

$$T_o = [\boldsymbol{G}_o^f]^T T_f, \tag{3}$$

where $T_o \in \mathscr{R}^{6\times 1}$ denotes the dynamic forces and moments in the three-dimensional operational space including the inertial load and external load. $T_f \in \mathscr{R}^{m.n_f\times 1}$ and

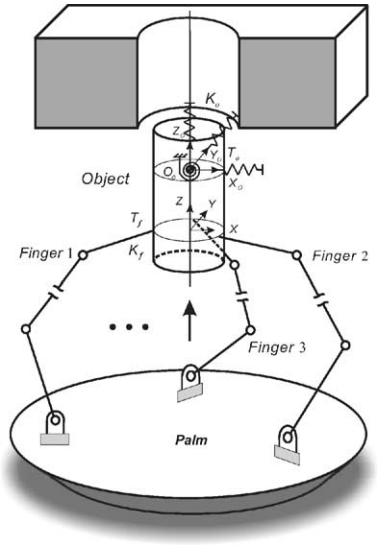

Fig. 5. Peg-in-hole task by using a multi-fingered hand.

$[\boldsymbol{G}_{\mathrm{o}}^{\mathrm{f}}] \in \mathscr{R}^{m.n_{\mathrm{f}}\times 6}$ denote the fingertip force vector in the fingertip space and the grasp Jacobian matrix, respectively. Here, m denotes the dimension of the wrench transmitted through each contact point [21].

To define the force transmission ratio between the operational space and the fingertip space, we first define the norm of the operational force, $\|T_{\mathrm{o}}\|$, and that of the fingertip space, $\|T_{\mathrm{f}}\|$, as follows:

$$\|T_{\mathrm{o}}\| = \{T_{\mathrm{o}}^{\mathrm{T}} T_{\mathrm{o}}\}^{1/2}, \tag{4}$$

$$\|T_{\mathrm{f}}\| = \{T_{\mathrm{f}}^{\mathrm{T}} T_{\mathrm{f}}\}^{1/2}. \tag{5}$$

Substituting (3) into (4), Eq. (4) can be rewritten as

$$\|T_{\mathrm{o}}\| = \{T_{\mathrm{f}}^{\mathrm{T}} [\boldsymbol{G}_{\mathrm{o}}^{\mathrm{f}}][\boldsymbol{G}_{\mathrm{o}}^{\mathrm{f}}]^{\mathrm{T}} T_{\mathrm{f}}\}^{1/2}. \tag{6}$$

Then, the force transmission ratio σ_{F} between the operational space and the fingertip space is expressed as

$$\sigma_{\mathrm{F}} = \frac{\|T_{\mathrm{o}}\|}{\|T_{\mathrm{f}}\|} = \left\{ \frac{T_{\mathrm{f}}^{\mathrm{T}} [\boldsymbol{G}_{\mathrm{o}}^{\mathrm{f}}][\boldsymbol{G}_{\mathrm{o}}^{\mathrm{f}}]^{\mathrm{T}} T_{\mathrm{f}}}{T_{\mathrm{f}}^{\mathrm{T}} T_{\mathrm{f}}} \right\}^{1/2}. \tag{7}$$

Using Rayleigh Quotient [14], the force in the operational space is bounded by

$$\lambda_{\min}\|T_{\mathrm{f}}\| \leqslant \|T_{\mathrm{o}}\| \leqslant \lambda_{\max}\|T_{\mathrm{f}}\|, \tag{8}$$

where $\lambda_{\min}$ and $\lambda_{\max}$ denote the minimum and maximum values of the square root of the singular value of $[\boldsymbol{G}_{\mathrm{o}}^{\mathrm{f}}][\boldsymbol{G}_{\mathrm{o}}^{\mathrm{f}}]^{\mathrm{T}}$, respectively.

Rearranging (8), we have

$$\bar{\sigma}_{\mathrm{F,min}}\|T_{\mathrm{o}}\| \leqslant \|T_{\mathrm{f}}\| \leqslant \bar{\sigma}_{\mathrm{F,max}}\|T_{\mathrm{o}}\|, \tag{9}$$

where

$$\bar{\sigma}_{\mathrm{F,min}} = \frac{1}{\lambda_{\max}}, \tag{10}$$

$$\bar{\sigma}_{\mathrm{F,max}} = \frac{1}{\lambda_{\min}} \tag{11}$$

and here, $\bar{\sigma}_{\mathrm{F,min}}$ and $\bar{\sigma}_{\mathrm{F,max}}$ denote the minimum and maximum force transmission ratios from the operational space to the fingertip space, respectively.

Thus, it is remarked that if the maximum force transmission ratio is minimized, the resultant load at the fingertip is minimized.

2.4. Task isotropy index

When an object is being manipulated by multi-fingered hands, the precise position or force control may not be guaranteed if any finger lies in the vicinity of singular positions. Isotropy index is useful to investigate the proper configuration of each finger for dextrous manipulation tasks. The task isotropy index is defined as

$$\sigma_{\mathrm{TI}} = \frac{\lambda_{\min}}{\lambda_{\max}}, \tag{12}$$

where $\lambda_{\min}$ and $\lambda_{\max}$ are determined by (8).

Specially, the task isotropy index approaches 1.0 at isotropic configuration and it is equal to zero at the singular grasp geometry. Thus, maximizing this index is desirable in the viewpoint of dexterity.

2.5. Stiffness mapping-based grasp isotropy index

The stiffness (or compliance) characteristic is a fundamental property for various contact tasks. Particularly, the stiffness characteristic can be employed for characterizing the grasping and manipulation of multi-fingered hands in the case that it is specially dominated in approximated linear analysis where low velocities and small relative motions lead to small inertial forces. Thus, we consider the stiffness mapping between the operational space and the fingertip space as one of grasp measures.

In general, grasping and manipulation of an object by multi-fingered hands is not easy due to the coupling among fingers and/or joints. If the coupling effect can be analyzed, control of fingers becomes easier. Recently, Kim et al. [15] presented an independent finger-based compliance control to eliminate the finger coupling effect. The stiffness relation between the operational space and the fingertip space can be expressed as

$$[\boldsymbol{K}_{\mathrm{o}}] = [\boldsymbol{G}_{\mathrm{o}}^{\mathrm{f}}]^{\mathrm{T}}[\boldsymbol{K}_{\mathrm{f}}][\boldsymbol{G}_{\mathrm{o}}^{\mathrm{f}}], \tag{13}$$

where the 6×6 operational stiffness matrix of $[\boldsymbol{K}_{\mathrm{o}}]$ including the effect of the change of grasp configuration in the three-dimensional space can be expressed as follows:

$$[\boldsymbol{K}_{\mathrm{o}}] = \left[\begin{array}{ccc|ccc} \boldsymbol{K}_{\mathrm{o}xx} & \boldsymbol{K}_{\mathrm{o}xy} & \boldsymbol{K}_{\mathrm{o}xz} & \boldsymbol{K}_{\mathrm{o}x\gamma} & \boldsymbol{K}_{\mathrm{o}x\beta} & \boldsymbol{K}_{\mathrm{o}x\alpha} \\ \boldsymbol{K}_{\mathrm{o}yx} & \boldsymbol{K}_{\mathrm{o}yy} & \boldsymbol{K}_{\mathrm{o}yz} & \boldsymbol{K}_{\mathrm{o}y\gamma} & \boldsymbol{K}_{\mathrm{o}y\beta} & \boldsymbol{K}_{\mathrm{o}y\alpha} \\ \boldsymbol{K}_{\mathrm{o}zx} & \boldsymbol{K}_{\mathrm{o}zy} & \boldsymbol{K}_{\mathrm{o}zz} & \boldsymbol{K}_{\mathrm{o}z\gamma} & \boldsymbol{K}_{\mathrm{o}z\beta} & \boldsymbol{K}_{\mathrm{o}z\alpha} \\ \hline \boldsymbol{K}_{\mathrm{o}\gamma x} & \boldsymbol{K}_{\mathrm{o}\gamma y} & \boldsymbol{K}_{\mathrm{o}\gamma z} & \boldsymbol{K}_{\mathrm{o}\gamma\gamma} & \boldsymbol{K}_{\mathrm{o}\gamma\beta} & \boldsymbol{K}_{\mathrm{o}\gamma\alpha} \\ \boldsymbol{K}_{\mathrm{o}\beta x} & \boldsymbol{K}_{\mathrm{o}\beta y} & \boldsymbol{K}_{\mathrm{o}\beta z} & \boldsymbol{K}_{\mathrm{o}\beta\gamma} & \boldsymbol{K}_{\mathrm{o}\beta\beta} & \boldsymbol{K}_{\mathrm{o}\beta\alpha} \\ \boldsymbol{K}_{\mathrm{o}\alpha x} & \boldsymbol{K}_{\mathrm{o}\alpha y} & \boldsymbol{K}_{\mathrm{o}\alpha z} & \boldsymbol{K}_{\mathrm{o}\alpha\gamma} & \boldsymbol{K}_{\mathrm{o}\alpha\beta} & \boldsymbol{K}_{\mathrm{o}\alpha\alpha} \end{array}\right]$$

where x, y, and z denote the operational positions, and α, β, and γ denote the rotational parameters. And $[\boldsymbol{K}_{\mathrm{f}}]$ denoting the fingertip stiffness matrix is given as

$$[\boldsymbol{K}_{\mathrm{f}}] = \begin{bmatrix} {}^{1}\boldsymbol{K}_{\mathrm{f}} & {}^{12}\boldsymbol{K}_{\mathrm{f}} & \cdots & {}^{1n_{\mathrm{f}}}\boldsymbol{K}_{\mathrm{f}} \\ {}^{21}\boldsymbol{K}_{\mathrm{f}} & {}^{2}\boldsymbol{K}_{\mathrm{f}} & \cdots & {}^{2n_{\mathrm{f}}}\boldsymbol{K}_{\mathrm{f}} \\ \vdots & \vdots & \ddots & \vdots \\ {}^{n_{\mathrm{f}}1}\boldsymbol{K}_{\mathrm{f}} & {}^{n_{\mathrm{f}}2}\boldsymbol{K}_{\mathrm{f}} & \cdots & {}^{n_{\mathrm{f}}}\boldsymbol{K}_{\mathrm{f}} \end{bmatrix},$$

in which $[{}^{i}\boldsymbol{K}_{\mathrm{f}}]$ $(i = 1, \ldots, n_{\mathrm{f}})$, denoting the stiffness matrix at the ith fingertip, is given by

$$[{}^{i}\boldsymbol{K}_{\mathrm{f}}] = \begin{bmatrix} {}^{i}\boldsymbol{K}_{\mathrm{f}xx} & {}^{i}\boldsymbol{K}_{\mathrm{f}xy} & {}^{i}\boldsymbol{K}_{\mathrm{f}xz} \\ {}^{i}\boldsymbol{K}_{\mathrm{f}yx} & {}^{i}\boldsymbol{K}_{\mathrm{f}yy} & {}^{i}\boldsymbol{K}_{\mathrm{f}yz} \\ {}^{i}\boldsymbol{K}_{\mathrm{f}zx} & {}^{i}\boldsymbol{K}_{\mathrm{f}zy} & {}^{i}\boldsymbol{K}_{\mathrm{f}zz} \end{bmatrix}.$$

In order to remove inter-finger coupling, all the off-diagonal terms of $[K_{\mathrm{f}}]$ should be null matrices. In [15], an alternative form of (13) is given by

$$K_{\mathrm{oo}} = [\boldsymbol{B}_{\mathrm{f}}^{\mathrm{o}}] K_{\mathrm{ff}}, \tag{14}$$

where K_{oo} and K_{ff} denote the independent stiffness elements in the operational and fingertip spaces, respectively. $[\boldsymbol{B}_{\mathrm{f}}^{\mathrm{o}}]$ denotes the stiffness mapping matrix between the operational space and the fingertip space. Note that the stiffness mapping matrix is a function of grasp geometry and consequently, the control performance can be changed according to the employed grasp geometry.

To evaluate the quality of the selected grasp points for effective compliant tasks, we define the stiffness mapping-based grasp isotropy index as follows:

$$\sigma_{\mathrm{SI}} = \frac{\lambda_{\mathrm{S,min}}}{\lambda_{\mathrm{S,max}}}, \tag{15}$$

where $\lambda_{\mathrm{S,min}}$ and $\lambda_{\mathrm{S,max}}$ denote the minimum and maximum values of the square root of the singular value of $[\boldsymbol{B}_{\mathrm{f}}^{\mathrm{o}}][\boldsymbol{B}_{\mathrm{f}}^{\mathrm{o}}]^{\mathrm{T}}$, respectively.

Using this index, a more proper grasp points on the given object can be determined for effective, precise assembly task such as a peg-in-hole as shown in Fig. 5.

3. Non-dimensionalized composite grasp index

The physical meanings of the grasp indices defined in Section 2 are different from each other. So, a generalized grasp index is necessary to evaluate a given grasp geometry. In this section, we present a non-dimensionalized composite grasp index that combines the grasp indices as one measure after normalizing each grasp index. The optimal grasp in this paper implies the grasp with the grasp points at which the non-dimensionalized composite grasp index is maximized.

In the literature, Terano et al. [16] and Wood [17] proposed a design procedure reflecting fuzzy algorithm. They employed a normalization procedure that rearranges each performance index from 0 to 1 as the task-based preference information. It can be usefully applied to obtain a non-dimensionalized performance measure for any physical performance index.

Since the stability grasp index, uncertainty grasp index, and maximum force transmission ratio index should be minimized for optimal grasping and manipulation tasks, their normalized indices can be defined as

$$\tilde{I}_{\mathrm{S}} = \frac{(I_{\mathrm{S}})_{\max} - I_{\mathrm{S}}}{(I_{\mathrm{S}})_{\max} - (I_{\mathrm{S}})_{\min}}, \tag{16}$$

$$\tilde{I}_{\mathrm{U}} = \frac{(I_{\mathrm{U}})_{\max} - I_{\mathrm{U}}}{(I_{\mathrm{U}})_{\max} - (I_{\mathrm{U}})_{\min}} \tag{17}$$

and

$$\tilde{I}_{\mathrm{F}} = \frac{(\bar{\sigma}_{\mathrm{F,max}})_{\max} - \bar{\sigma}_{\mathrm{F,max}}}{(\bar{\sigma}_{\mathrm{F,max}})_{\max} - (\bar{\sigma}_{\mathrm{F,max}})_{\min}}, \tag{18}$$

where $\tilde{I}_{\mathrm{S}}$ and $\tilde{I}_{\mathrm{U}}$ denote the normalized stability and uncertainty grasp indices, respectively, and $\tilde{I}_{\mathrm{F}}$ denotes the normalized maximum force transmission ratio index. In (16)–(18), $(\cdot)_{\max}$ and $(\cdot)_{\min}$ denote the maximum and minimum values for all the candidates of the corresponding performance indices, respectively. Physically, those mean the boundary conditions for the feasible grasp region.

On the other hand, the task isotropy index and the stiffness mapping-based grasp index are desirable to be maximized for dextrous manipulation tasks. Thus, those indices can be normalized as follows, respectively,

$$\tilde{I}_{\mathrm{T}} = \frac{\sigma_{\mathrm{TI}} - (\sigma_{\mathrm{TI}})_{\min}}{(\sigma_{\mathrm{TI}})_{\max} - (\sigma_{\mathrm{TI}})_{\min}} \tag{19}$$

and

$$\tilde{I}_{\mathrm{SI}} = \frac{\sigma_{\mathrm{SI}} - (\sigma_{\mathrm{SI}})_{\min}}{(\sigma_{\mathrm{SI}})_{\max} - (\sigma_{\mathrm{SI}})_{\min}}, \tag{20}$$

where $\tilde{I}_{\mathrm{T}}$ and $\tilde{I}_{\mathrm{SI}}$ denote the normalized task isotropy and stiffness mapping-based isotropy indices, respectively. In (19) and (20), $(\cdot)_{\max}$ and $(\cdot)_{\min}$ denote the maximum and minimum values for all the candidates of the corresponding performance indices, respectively.

Through the analysis, we define a non-dimensionalized composite grasp index I_G that evaluates the selected grasp geometry by aggregating all the individual grasp indices as one measure. The non-dimensionalized composite grasp index is as follows:

$$I_{\mathrm{G}} = \min\{(\tilde{I}_{\mathrm{S}})^{w_1}, (\tilde{I}_{\mathrm{U}})^{w_2}, (\tilde{I}_{\mathrm{F}})^{w_3}, (\tilde{I}_{\mathrm{T}})^{w_4}, (\tilde{I}_{\mathrm{SI}})^{w_5}\}, \tag{21}$$

where w_i $(i = 1, 2, \ldots, 5)$ denote the weighting factors and those can be set as greater than or equal to 1.0 as the standpoint of the given tasks.

Then, we construct the data base of the proposed weighted composite grasp index by selecting the minimum values of all normalized grasp indices for each grasp point. Finally, we can obtain the optimal grasp points by choosing the grasp that has the largest weighted composite grasp index in the data base.

4. Simulation study

In this section, we show the feasibility of the proposed optimal grasp search method by simulations. Particularly, we consider two examples of assembly tasks using multi-fingered hands. For performing any manipulating tasks using multi-fingered hands, it is necessary to investigate the finger condition of hands. Fundamental finger condition of multi-fingered hands has been analyzed in terms of compliance control [15]. The result illustrates that a two-dimensional compliant

works can be effectively achieved by using a three-fingered hand. Therefore, we use a three-fingered hand for evaluating the usefulness of the proposed optimal grasping index.

4.1. Optimal grasping for a peg-in-hole task

The objective of the first application is to search the optimal grasp position for a simple peg-in-hole task using a three-fingered hand in two-dimensional space as shown in Fig. 6 and then discuss the characteristics of the grasp indices, proposed in Section 2, by using the grasp polygon.

Since the distal part of the peg in Fig. 6 should be inserted into the hole, the expectable grasp positions of each finger will be the remaining three sides of the peg. However, some cases of all possible grasp candidates may not be accepted by the kinematical and/or dynamical constraints of the hand. Thus, in this example, consider the case that each finger grasps one of the three sides and the feasible grasp ranges of each finger are given in Table 1 during the insertion task, where the x- and y-directional coordinates denote the distances from the operational space to the fingertip space in Fig. 6(a). Practically, it is possible to check the feasible grasp region

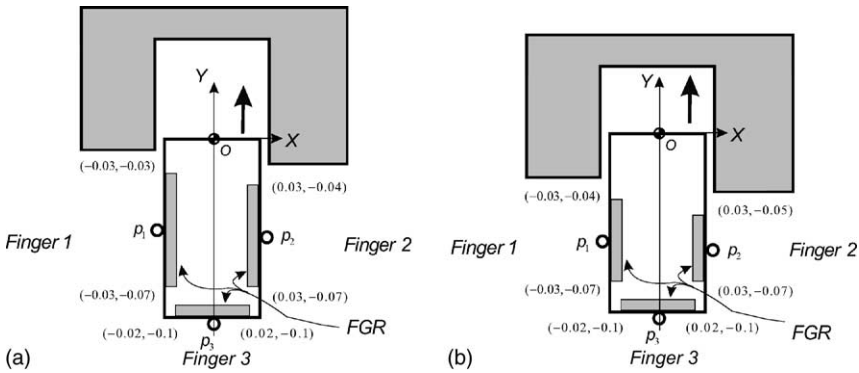

Fig. 6. Peg-in-hole task by using a three-fingered hand.

Table 1
Grasp region of each finger (unit: m)

Finger	x-axis		y-axis		Reference
	Initial	End	Initial	End	
1	−0.03	−0.03	−0.07	−0.03	
2	0.03	0.03	−0.07	−0.04	Fig. 6(a)
3	−0.02	−0.02	−0.1	−0.1	
1	−0.03	−0.03	−0.07	−0.04	
2	0.03	0.03	−0.07	−0.05	Fig. 6(b)
3	−0.02	−0.02	−0.1	−0.1	

for each finger during the task. Also, in order to stably maintain the grasp during the assembly task, the internal forces applied to the object by three fingers should satisfy the force closure relation [10,23]. To be specific, the x-directional internal forces in Fig. 6 are determined by

$$ {}^1f_{\mathrm{f}x,\mathrm{int}} + {}^2f_{\mathrm{f}x,\mathrm{int}} + {}^3f_{\mathrm{f}x,\mathrm{int}} = 0, \tag{22} $$

where

$$ {}^1f_{\mathrm{f}x,\mathrm{int}} = {}^1\boldsymbol{K}_{\mathrm{f}xx}\delta^1 x_{\mathrm{f}x,\mathrm{int}}, $$
$$ {}^2f_{\mathrm{f}x,\mathrm{int}} = {}^2\boldsymbol{K}_{\mathrm{f}xx}\delta^2 x_{\mathrm{f}x,\mathrm{int}} $$

and

$$ {}^3f_{\mathrm{f}x,\mathrm{int}} = {}^3\boldsymbol{K}_{\mathrm{f}xx}\delta^3 x_{\mathrm{f}x,\mathrm{int}}. $$

In (22), the definition of ${}^if_{\mathrm{f}x,\mathrm{int}}$ and ${}^i\boldsymbol{K}_{\mathrm{f}xx}$ denote the x-directional internal force and fingertip stiffness for the ith finger, respectively. And $\delta^i x_{\mathrm{f}x,\mathrm{int}}$ denotes the displacement in the fingertip space to consider the corresponding internal forces for the ith finger.

The y-directional internal forces in Fig. 6 are determined by

$$ {}^1f_{\mathrm{f}y,\mathrm{int}} + {}^2f_{\mathrm{f}y,\mathrm{int}} + {}^3f_{\mathrm{f}y,\mathrm{int}} = 0, \tag{23} $$

where

$$ {}^1f_{\mathrm{f}y,\mathrm{int}} = {}^1\boldsymbol{K}_{\mathrm{f}yy}\delta^1 y_{\mathrm{f}y,\mathrm{int}}, $$
$$ {}^2f_{\mathrm{f}y,\mathrm{int}} = {}^2\boldsymbol{K}_{\mathrm{f}yy}\delta^2 y_{\mathrm{f}y,\mathrm{int}} $$

and

$$ {}^3f_{\mathrm{f}y,\mathrm{int}} = {}^3\boldsymbol{K}_{\mathrm{f}yy}\delta^3 y_{\mathrm{f}y,\mathrm{int}}. $$

In (23), the definition of ${}^if_{\mathrm{f}y,\mathrm{int}}$ and ${}^i\boldsymbol{K}_{\mathrm{f}yy}$ denote the y-directional internal force and fingertip stiffness for the ith finger, respectively. And $\delta^i y_{\mathrm{f}y,\mathrm{int}}$ denotes the displacement in the fingertip space to consider the corresponding internal forces for the ith finger.

Also, the magnitude of internal forces are decided in such a way to satisfy friction cone constraint at the contact point of each finger.

In this simulation, all grasp candidates formed by three points are uniquely given and those are validated by comparing the non-dimensionalized composite grasp index. Also, the weighting factors w_i $(i = 1, \ldots, 5)$ in (21) are set as 1.0, 1.5, 1.0, 1.0, 1.0, respectively. To be specific, the weighting factor of the uncertainty grasp index is set relatively greater than the others. This implies that the uncertainty grasp performance can be dominantly considered for precise insertion of the peg. From Fig. 7, we can find that the 1149th grasp sample is illustrated as the optimal grasp at the beginning of the given task as shown in Fig. 6(a). Particularly, the optimal grasp position $p_i(x, y)$ for the ith finger is as follows: $p_1(x, y) = (-0.03, -0.034)$, $p_2(x, y) = (0.03, -0.055)$, and $p_3(x, y) = (0.0, -0.1)$. During the inserting task, if the feasible grasp range of each finger is changed as shown in Table 1, the corresponding optimal grasp positions for all fingers are determined as $p_1(x, y) = (-0.03, -0.043)$, $p_2(x, y) = (0.03, -0.06)$, and $p_3(x, y) = (0.0, -0.1)$. As a result, we can notice that in

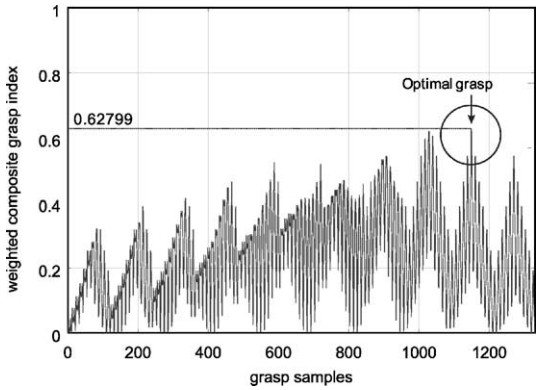

Fig. 7. Non-dimensionalized composite grasp index for all grasp points.

the insertion task of the peg, the optimal grasp position moves towards the opposite direction of the peg insertion and also it can be naturally experienced in human grasping.

Now, consider the optimal grasp polygon formed by the optimal grasp points for all fingers and the neighborhood of the optimal grasp to confirm the trend of the proposed grasp indices. When the feasible grasp region for each finger is given by Fig. 8, the normalized grasp indices for all the selected grasp polygons can be shown in Fig. 9. Table 2 presents the evaluated composite grasp indices for the selected grasp polygons in near the optimal grasp, where the positions (x, y) of fingers 1 and 3 are $(-0.03, -0.034)$ and $(0.0, -0.1)$, respectively. From Table 2, we can notice that the polygon $p_1p_{2c}p_3$ is the optimal grasp polygon, which is coincident to intuition. Also, note that the normalized grasp index of the grasp polygon $p_1p_{2a}p_3$ is accidentally the same as that of the grasp polygon $p_1p_{2e}p_3$. However, even though the

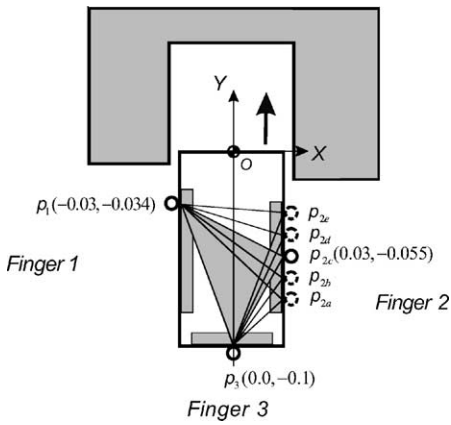

Fig. 8. Grasp points and polygons.

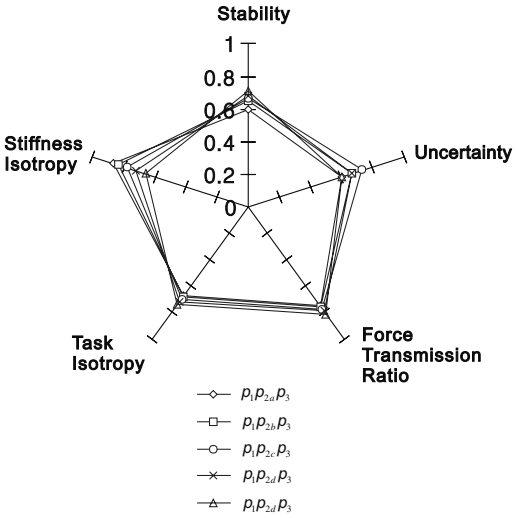

Fig. 9. Normalized grasp indices as the grasp configurations.

Table 2
Evaluated weighted grasp index for each grasp polygon

Grasp polygon	Pos. of finger 2 (x, y) [m]	I_G	Reference
$p_1p_{2a}p_3$	0.03, −0.061	0.465	
$p_1p_{2b}p_3$	0.03, −0.058	0.544	
$p_1p_{2c}p_3$	0.03, −0.055	0.628	Fig. 8
$p_1p_{2d}p_3$	0.03, −0.052	0.544	
$p_1p_{2e}p_3$	0.03, −0.049	0.465	

normalized grasp indices are identical, the individual grasp index may differ from each other. Specifically, the normalized grasp indices for the grasp polygons are illustrated in Table 3. From Fig. 9 and Table 3, we can observe that the stiffness isotropy is the largest in the grasp polygon $p_1p_{2a}p_3$, and the grasp polygon $p_1p_{2c}p_3$ has the largest uncertainty grasp index. The other indices have the largest values in the grasp polygon $p_1p_{2e}p_3$.

Table 3
Normalized grasp indices for each grasp polygon

Grasp polygon	$\tilde{I}_S$	$\tilde{I}_U$	$\tilde{I}_F$	$\tilde{I}_T$	$\tilde{I}_{SI}$
$p_1p_{2a}p_3$	0.594	0.600	0.746	0.671	0.868
$p_1p_{2b}p_3$	0.647	0.667	0.755	0.683	0.831
$p_1p_{2c}p_3$	0.662	0.733	0.769	0.698	0.782
$p_1p_{2d}p_3$	0.682	0.667	0.785	0.718	0.723
$p_1p_{2e}p_3$	0.708	0.600	0.805	0.743	0.658

Consequently, it is concluded that the grasp polygon $p_1p_{2c}p_3$ is selected as the optimal grasp polygon in viewpoint of the uncertainty grasp index. This shows the natural trend of grasp planning by employing a larger weighting for the uncertainty grasp performance index than the others. Also, we can recognize that all grasp indices of the grasp polygon $p_1p_{2c}p_3$ are well-balanced in comparison to the others. Specifically, since the position of finger 2 is located at the nearest center of the feasible grasp region, it is natural to have the largest uncertainty grasp index in the grasp polygon $p_1p_{2c}p_3$. Table 3 also shows that there exists a trade-off between grasp indices. So, various performance indices should be properly combined to obtain the optimal grasp for dextrous grasping and manipulation tasks.

4.2. Optimal grasping for an L-typed peg-in-hole task

In the second simulation, we analyze the selection of optimal grasp positions for an irregular peg-in-hole task using the same hand. In fact, it is shown that the optimal grasp for the given task may be changed according to the weighting factors of the performance indices.

Consider that in an L-typed peg as shown in Fig. 10(a), the defined grasp positions c_i $(i = 1, \ldots, 6)$ can be determined as a grasp by multi-fingered hands. Particularly, in the case that a three-fingered hand grasps the defined grasp positions of the object, there exists 120 candidates of a grasp configuration. However, all of those grasp configurations may not be reliable because the configuration of the hand may not be available.

Now, let us consider an L-typed peg-in-hole task as shown in Fig. 10(b). For this task, the positions denoted by c_1, c_2, and c_3 in Fig. 10(a) are desirable. By the way, we have 6 degree-of-freedoms to grasp the object. So, the feasible grasp region for each finger is checked a priori. Also, note that the feasible grasp region of finger 2 may be limited because the finger 2 is possible to collide with the under-edge of the hole. In many cases, typical assembly examples can be similarly formed by this task. And the control performance of this assembly task is more sensitive than the case of

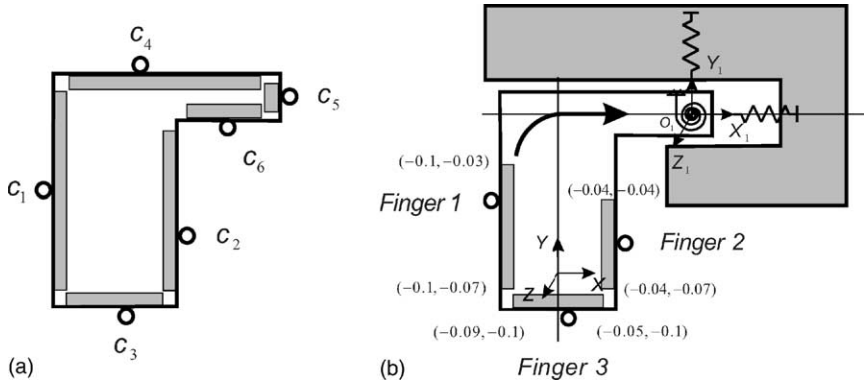

Fig. 10. Peg-in-hole task with L-type object.

the straight peg-in-hole task due to the torque effect and the limited grasp region. Recently, in order to improve the performance of assembly tasks, an analytical research considering the compliance center and the torque effect has been presented [22]. Additionally, this paper considers an optimal grasp planning for effective assembly tasks. Here, we shows that an optimal grasp planning plays an important role to improve the performance of typical peg-in-hole tasks. Then, in order to find the optimal grasp positions for the preference of the given task, we try to find the optimal grasp positions according to the weighting factors.

Table 4 illustrates the optimal grasp positions according to the specified weighting factors. Since the weighting factor means the preference of the given task, it is possible to search the optimal grasp by properly selecting the weighting factor of each performance index. In Table 4, x_j and y_j denote the x- and y-directional coordinates, which represent the distances from the operational space $\boldsymbol{O}_1$ to the fingertip space in Fig. 10. And the factor w_i $(i = 1, \ldots, 5)$ means the corresponding weighting given in (21). In Fig. 10, the current grasp positions of the fingers represent the optimal grasp positions when employing the same weighting factors for all grasp indices. Here, this grasp is the initial grasp. From Table 4, when the weighting factor w_1 for the stability grasp index is only increased as 4.0, it is seen that the third finger moves to the negative x-direction. Thus, the grasped geometry approaches to the shape of regular polygon and this represents more stable configuration. Also, we can observe that the first finger moves downward from the current grasp position if the

Table 4
Optimal grasp positions by using the weighting factors

Weighting factors w_i $(i = 1, \ldots, 5)$	Grasp positions [m]		I_G
	j	x_j, y_j	
1.0, 1.0, 1.0, 1.0, 1.0	1	−0.1, −0.038	0.6184
	2	−0.04, −0.055	
	3	−0.066, −0.1	
4.0, 1.0, 1.0, 1.0, 1.0	1	−0.1, −0.038	0.6105
	2	−0.04, −0.055	
	3	−0.078, −0.1	
1.0, 4.0, 1.0, 1.0, 1.0	1	−0.1, −0.046	0.4671
	2	−0.04, −0.055	
	3	−0.066, −0.1	
1.0, 1.0, 4.0, 1.0, 1.0	1	−0.1, −0.03	0.5058
	2	−0.04, −0.055	
	3	−0.066, −0.1	
1.0, 1.0, 1.0, 4.0, 1.0	1	−0.1, −0.03	0.4409
	2	−0.04, −0.052	
	3	−0.062, −0.1	
1.0, 1.0, 1.0, 1.0, 4.0	1	−0.1, −0.03	0.5059
	2	−0.04, −0.055	
	3	−0.066, −0.1	

weighting factor w_2 for the uncertainty grasp index is relatively large. Since the more a grasp position lies near the center of each feasible grasp region, the more the position sensitivity is insensible. Thus, this trend is naturally experienced in human grasping.

On the other hand, in order to select the optimal grasp position with respect to the force transmission ratio or stiffness mapping-based grasp indices, it is pointed out that the first finger should grasp the upper position from the initial grasp. In fact, this configuration is adequate to support large operational forces in the assembly task in comparison to the previous case. In terms of compliant inserting, the second finger is desirable to move the grasp to the downward position from the initial grasp and the third finger to the left direction, while the case of focusing the effective force transmission requires the reverse. Therefore, there exists somewhat a trade-off between the two indices. Consequently, it is concluded that the optimal grasp positions according to the viewpoint of the given task can be properly obtained by employing the weighting factors.

4.3. Task-based optimal grasp planning

In practical applications, the manipulation task of an object by multi-fingered hands can be associated with many control problems such as trajectory control, force control, and hybrid control. For example, let us consider a manipulating task interacting with an environment by a three-fingered robot hand as shown in Fig. 11. The task is a typical example including trajectory control, force control, and hybrid control phases. Based on the objective of the given task, we can consider some grasp

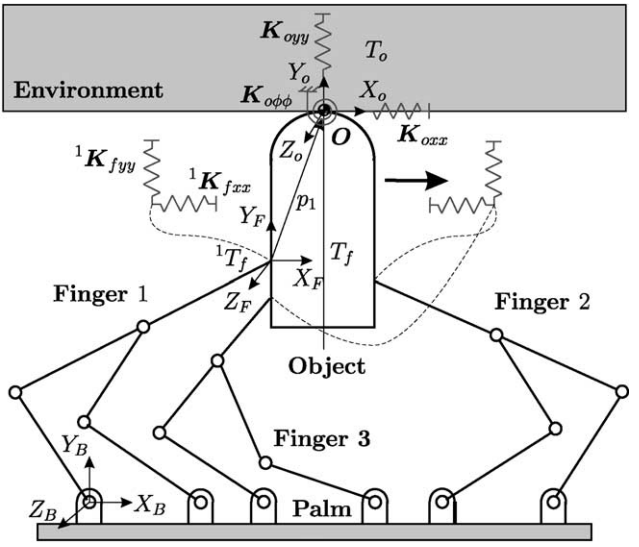

Fig. 11. Compliant contact task by a three-fingered hand.

Table 5
Task-based grasp configuration

Task	Preference of grasp indices*					Grasp configuration
	I_S	I_U	I_F	I_T	I_{SI}	
Trajectory control	□	○	△	△	–	Fig. 13(a)
Force control	△	□	△	△	○	Fig. 13(b)
Hybrid control	□	○	△	△	□	Fig. 13(c)

* It represents the priority of the defined indices for the given task (○ > □ > △).

indices as the principal performance measure of the task. In this sense, Table 5 denotes the preferences of the grasp indices. In Table 5, each priority of the symbols, ○, □, and △, has been assigned as 6.0, 3.0, and 1.0, respectively. The optimal grasp configuration is determined through the same procedure of the previous simulations. Specifically, Fig. 12(a)–(e) show the trend of the weighted grasp indices after normalizing on the hybrid control phase of the compliant task. From Fig. 12(b), we can confirm that a particular grasp configuration can be uniquely determined by the uncertainty grasp index. The trend of the maximum force transmission ratio and the task isotropy indices is similar in this case. Those indices are dependent on the grasp structure of the hand. On the other hand, many grasp candidates may have the similar grade case stiffness isotropy. Thus, the proposed non-dimensionalized composite grasp index can be usefully applied to combine all of the grasp indices as one measure. Specifically, we can find an optimal grasp through the evaluation of all indices by using a normalizing and weighting technique. As a result, by evaluating the proposed grasp index, the optimal grasp for the given task can be found from Fig. 12(f). The same procedure is applied to trajectory control and force control. Fig. 13 shows optimal grasp configurations for the three cases. It is observed that the case of force control tends to use a large moment arm between finger 1 and finger 2 for ensuring a firm grasp. On the other hand, the case of trajectory control is on the contrary. Also note that the hybrid control is in-between.

Additionally, Fig. 14 shows the resultant optimal grasp configuration for a hybrid control task by a four-fingered robot hand. This result was also evaluated based the same priority of the hybrid control task by the three-fingered hand.

Through the analysis, the trend of the defined various grasp indices are investigated through the typical examples for searching the optimal grasp. It is shown that we can effectively choose the desired optimal grasp positions by applying some weighting factors for the given task. So, the proposed non-dimensionalized composite grasp index is a task-based grasp index. Also, we can notice that the resultant trend of the proposed optimal grasp planning is coincident to the physical sense of human grasping. Since the proposed grasp index is based on the non-dimensionalizing technique of unifying different physical meanings, it can be easily expanded when another indices for some other requirements such as form closure grasp are needed. For real implementation, a sensor-based regrasping strategy is desirable to maintain the force equilibrium of the grasp and improve the quality of the grasp for effective manipulating tasks [24–27].

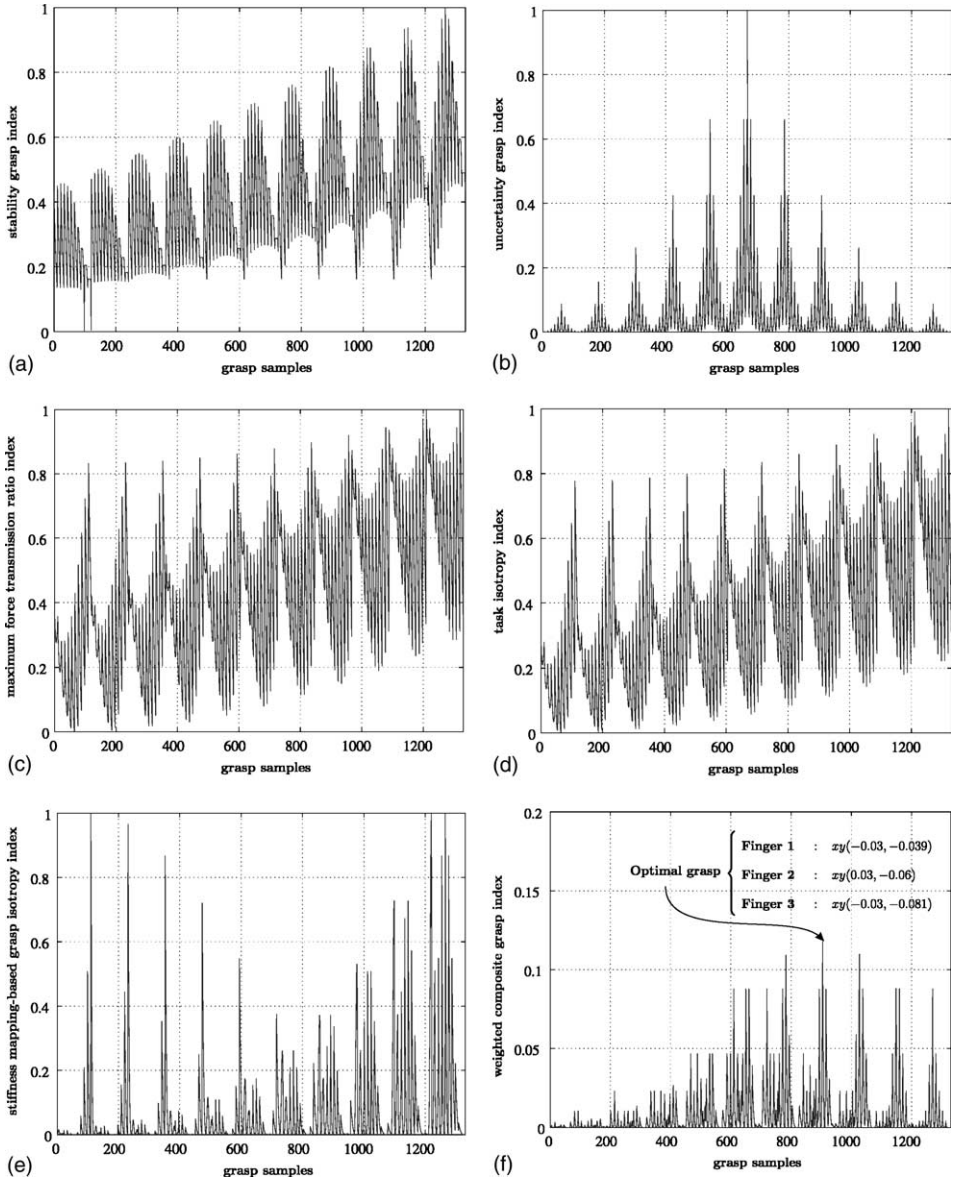

Fig. 12. The trend of the weighted grasp indices after normalizing on hybrid control.

5. Implementation of a hybrid control task

This section implements a hybrid control task by a three-fingered robot hand as shown in Fig. 11 and here a compliance control scheme developed in [15] is employed. In order for experimental work, we developed a three-fingered robot hand

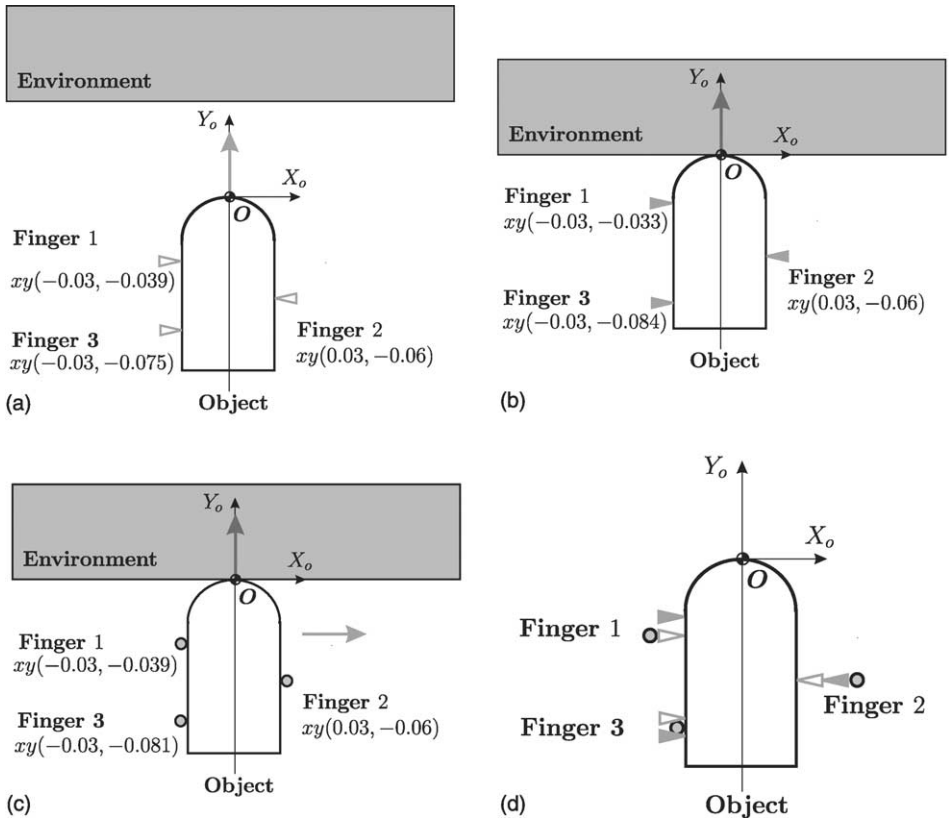

Fig. 13. Optimal grasp configuration for the given task.

driven by DC motors (Model No. DC-Micromotors 2343-024CR, MicroMo Electronics Inc.) with an encoder (Model No. HEDM 5500B, MicroMo Electronics Inc.) as shown in Fig. 15. Also, we developed a PC-based hand control system as shown in Fig. 16 for the hand.

In this experiment, the given task of the object, is to control the position along the x-direction and to control the force in the y-direction, where the grasped object is made of wood. The optimal grasping positions depicted on Fig. 13(c) are employed. The contact force to the y-direction is set as 3.0 N and the x-directional velocity of the grasped object as 0.000417 m/s, while controlling the orientation angle as 90°. Thus, the grasped object is to move along the x-direction while applying a certain level of force to the direction normal to the contact surface. The block diagram for the task is shown in Fig. 17. In Fig. 17, *RIFDS* is to decompose the desired compliance characteristic specified in the operational space into the compliance characteristic in the fingertip space without inter-finger coupling, and *RIJDS* is also to decompose the compliance characteristic in the fingertip space without inter-joint coupling [15]. The definition of ${}^{i}f_{\mathrm{fx,int}}$ and ${}^{i}f_{\mathrm{fy,int}}$ denote the x- and y-directional

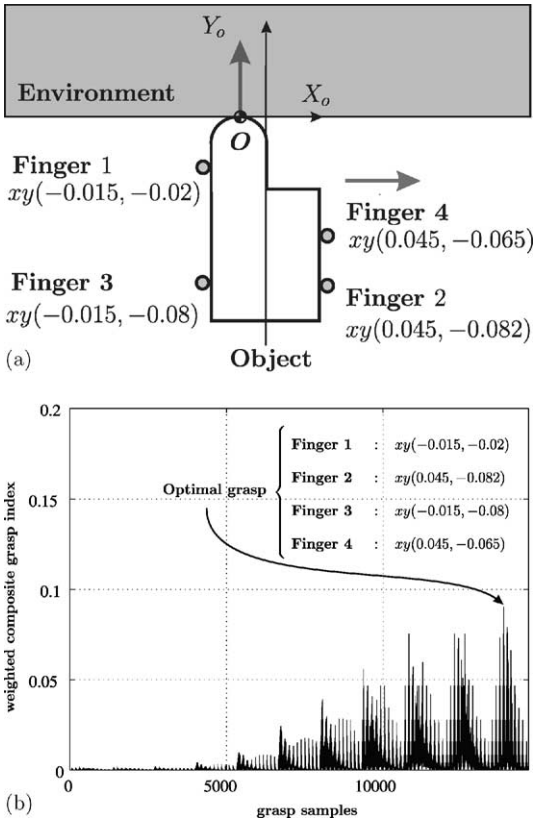

Fig. 14. Optimal grasp planning by a four-fingered robot hand.

internal force for the ith finger, respectively. In order to stably maintain the grasp during the contact task, the internal forces have been applied to the object by three fingers. To be specific, the x-directional internal forces are determined by

$$ {}^1f_{\mathrm{f}x,\mathrm{int}} + {}^2f_{\mathrm{f}x,\mathrm{int}} + {}^3f_{\mathrm{f}x,\mathrm{int}} = 0, \tag{24} $$

where

$$ {}^1f_{\mathrm{f}x,\mathrm{int}} = {}^1\boldsymbol{K}_{\mathrm{f}xx}\delta^1 x_{\mathrm{f}x,\mathrm{int}}, $$
$$ {}^2f_{\mathrm{f}x,\mathrm{int}} = {}^2\boldsymbol{K}_{\mathrm{f}xx}\delta^2 x_{\mathrm{f}x,\mathrm{int}} $$

and

$$ {}^3f_{\mathrm{f}x,\mathrm{int}} = {}^3\boldsymbol{K}_{\mathrm{f}xx}\delta^3 x_{\mathrm{f}x,\mathrm{int}}. $$

The y-directional internal forces are determined by

$$ {}^1f_{\mathrm{f}y,\mathrm{int}} + {}^2f_{\mathrm{f}y,\mathrm{int}} + {}^3f_{\mathrm{f}y,\mathrm{int}} = 0, \tag{25} $$

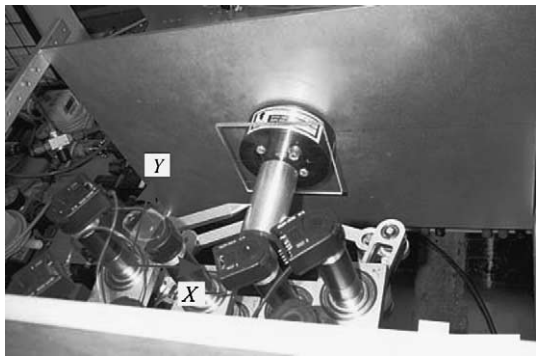

Fig. 15. Implementation of a compliant manipulating task.

Fig. 16. Developed PC-based hand control system.

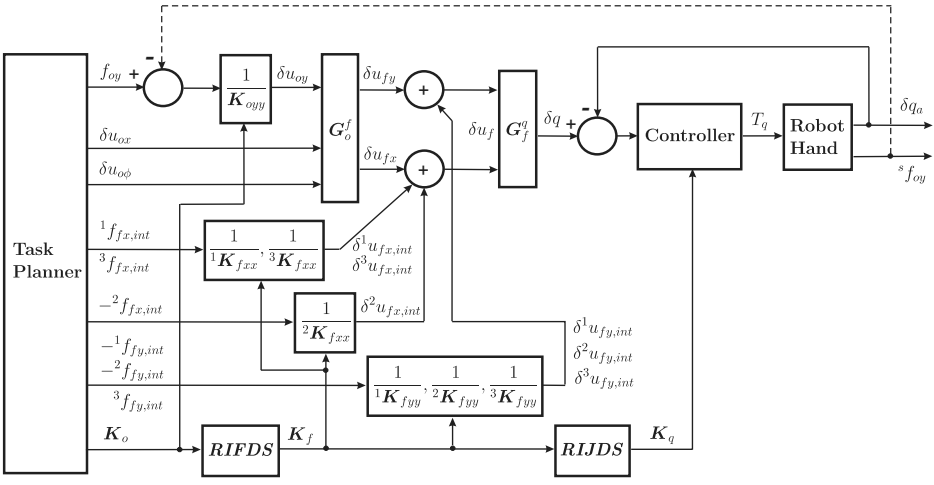

Fig. 17. Block diagram for the hybrid control.

where

$${}^1f_{\mathrm{f}y,\mathrm{int}} = {}^1\boldsymbol{K}_{\mathrm{f}yy}\delta^1 y_{\mathrm{f}y,\mathrm{int}},$$

$${}^2f_{\mathrm{f}y,\mathrm{int}} = {}^2\boldsymbol{K}_{\mathrm{f}yy}\delta^2 y_{\mathrm{f}y,\mathrm{int}}$$

and

$${}^3f_{\mathrm{f}y,\mathrm{int}} = {}^3\boldsymbol{K}_{\mathrm{f}yy}\delta^3 y_{\mathrm{f}y,\mathrm{int}}.$$

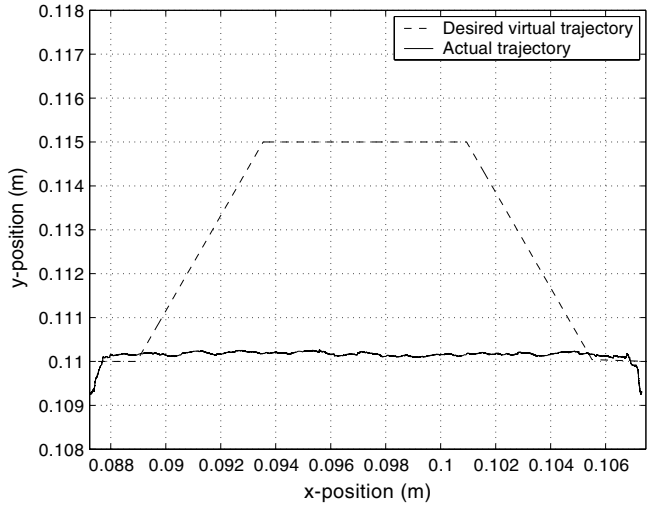

Fig. 18. Trajectory of the manipulated object.

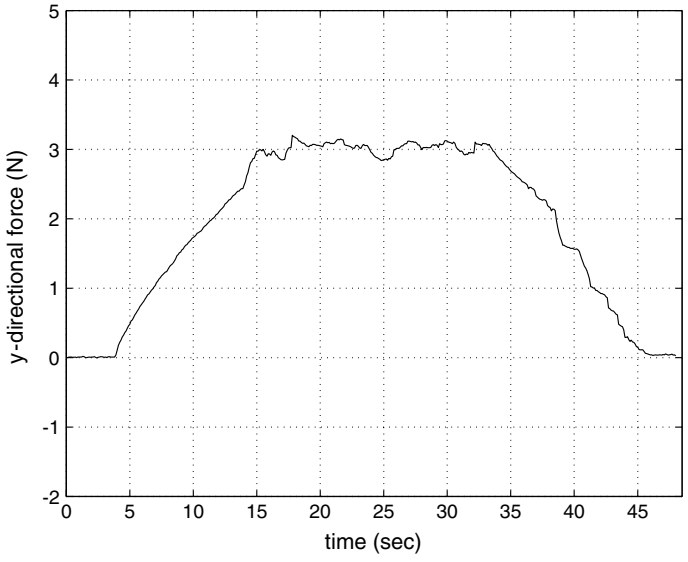

Fig. 19. History of the y-directional force applied to the environment.

Also, the magnitude of the internal forces are decided in such a way as to satisfy the friction cone constraint at the contact point of each finger.

In this work, we assign a proper stiffness in the operational space as follows:

$$[\boldsymbol{K}_{\mathrm{o}}] = \begin{bmatrix} 3000 & 0 & 120 \\ 0 & 600 & 0 \\ 120 & 0 & 18 \end{bmatrix} \ [\mathrm{N/m}] \tag{26}$$

for the optimal grasp positions, such as $y_1 = -0.039$ m, $y_2 = -0.06$ m, $y_3 = -0.081$ m, $x_1 = -0.03$ m, $x_2 = 0.03$ m, and $x_3 = -0.03$ m, evaluated in Section 4.3.

The performances of position and force tracking are shown to be satisfactory in Figs. 18 and 19. The trajectory of the grasped object lies on the surface of the contacting wall. Also, the interaction force of the object, during the constrained motion phase of the task, is shown to be properly followed according to the given motion trajectory in the y-direction.

6. Concluding remarks

Grasp planning is a fundamental topic in applications of multi-fingered hands. Thus, many researches for optimal grasp planning have been reported in the previous decade and many useful grasp indices are developed for dextrous grasping and manipulation tasks. Despite many years of research effort for optimal grasp planning, the reported grasp performance indices are not effectively combined as a unified measure to estimate a grasp for grasping and manipulation tasks. In fact, since the physical meanings of the defined grasp indices are different from each other, it is not easy to combine those indices to identify the optimal grasping. In this paper, various individual grasp indices are properly defined by considering the stability, uncertainty, and task-oriented performance characteristic. And then, a new generalized grasping performance index to represent all of the grasp indices as one unified measure is formulated by using a non-dimensionalizing technique. Also, optimal grasp planning based on the proposed grasp index is applied to determine the optimal grasp positions for maximizing the desired performances of the given task.

Through the task-based simulation studies using multi-fingered hands, the usefulness of the developed each grasp index is confirmed by applying it to evaluate the quality of each feasible grasp. And it is shown that the trend of the proposed optimal grasp planning is coincident to the physical sense of human grasping. Furthermore, some experimental results showing the task specific performances are incorporated to corroborate the effectiveness of the proposed optimal grasp planning algorithms. Since the proposed grasp index is based on the non-dimensionalizing technique unifying different physical meanings, it is easy to incorporate some other indices. Conclusively, the proposed optimal grasp planning can be applied to determine the optimal grasp positions for stable grasping and manipulation tasks using multi-fingered hands or multi-chained mechanisms.

Acknowledgements

This work was supported by the research fund of Hanyang University (HY-2002-S) and partially supported by Biomimetic Control National Research lab program sponsored by Ministry of Science and Technology, KOREA.

References

[1] Li Z, Hsu P, Sastry S. Grasping and coordinated manipulation by a multi-fingered robot hand. Int J Robot Res 1989;8(4):33–49.
[2] Yoshikawa T, Zheng X-Z. Coordinated dynamic hybrid position/force control for multiple robot manipulators handling one constrained object. Int J Robot Res 1993;12(3):219–30.
[3] Nagai K, Yoshikawa T. Grasping and manipulation by arm/multifingered-hand mechanisms. In: Proc of IEEE Int Conf on Robotics and Automation. 1995. p. 1040–7.
[4] Hasegawa T, Matsuoka T, Kiriki T, Honda K. Manipulation of an object by a multi-fingered hand with multi-sensors. In: Proc of the Int Conf on Industrial Electronics, Control, and Instrumentation. 1996. p. 174–9.
[5] Maekawa H, Tanie K, Komoria K. Dynamic grasping force control using tactile feedback for grasp of multifingered Hand. In: Proc of IEEE Int Conf on Robotics and Automation. April 1996. p. 2462–9.
[6] Maekawa H. Grasp and manipulation by a multifingered hand using tactile information. In: Proc of the 32nd Int Symposium on Robotics. April 2001. p. 790–5-2.
[7] Li Z, Sastry S. Task oriented optimal grasping by multifingered robot hands. In: Proc of IEEE Int Conf on Robotics and Automation. 1987. p. 389–94.
[8] Cutkosky MR. On grasp choice, grasp models, and the design of hands for manufacturing tasks. Trans Robot Autom 1989;5(3):269–79.
[9] Park YC, Starr GP. Optimal grasping using a multifingered robot hand. In: Proc of IEEE Int Conf on Robotics and Automation. 1990. p. 689–94.
[10] Park YC, Starr GP. Grasp synthesis of polygonal objects using three-fingered robot hand. Int J Robot Res 1992;11(3):163–84.
[11] Kaneko M, Tanie K. Contact point detection for grasping an unknown object using self-posture changeability. IEEE Trans Robot Autom 1994;10(3):355–67.
[12] You J-H, Park J-H, Choi D-H, Chong NY. Optimal grasp design of a multi-fingered robot hand based on manipulability and stability. Trans Korea Soc Mech Eng (A) 1998;22(7):1367–74.
[13] Lin Q, Burdick J-W, Rimon E. A stiffness-based quality measure for compliant grasps and fixtures. IEEE Trans Robot Autom 2000;16(6):675–88.
[14] Strang G. Linear algebra and its applications. Harcourt Brace Jovanovich, Inc.; 1988.
[15] Kim B-H, Yi B-J, Suh IH, Oh S-R. A biomimetic compliance control of robot hand by considering structures of human finger. In: Proc of IEEE Int Conf on Robotics and Automation. 2000. p. 3880–7.
[16] Terano T, Asai K, Sugeno M. Fuzzy systems theory and its applications. Academic Press, Inc, Harcourt Brace Jovanovich Publishers; 1992.
[17] Wood KL. A method for the representation and manipulation of uncertainties in preliminary engineering design. PhD Dissertation, Dept of Mechanical Eng, California Institute of Technology, 1989.
[18] Stanley K, Wu J, Jerbi A, Gruver WA. A fast two dimensional image based grasp planner. In: Proc of IEEE Int Conf on Intelligent Robots and Systems. 1999. p. 266–71.
[19] Hauck A, Rüttinger J, Sorg M, Färber G. Visual determination of 3D grasping points on unknown objects with a binocular camera system. In: Proc of IEEE/RSJ Int Conf on Intelligent Robots and Systems. 1999. p. 272–7.
[20] Sugiuchi H, Watanabe S, Morino T, Fukuno R. A control system for multi-fingered dual robotic hand with distributed touch sensor. In: Proc of the 32nd Int Symposium on Robotics. April 2001. p. 1255–9.

[21] Mason MT, Salisbury JK. Robot hands and the mechanics of manipulation. Cambridge: The MIT Press; 1985.
[22] Kim B-H, Yi B-J, Suh IH, Oh S-R. Stiffness analysis for effective peg-in-hole tasks using multi-fingered robot hands. In: Proc of IEEE/RSJ Int Conf on Intelligent Robots and Systems. 2000. p. 1229–36.
[23] Ponce J, Sullivan S, Sudsang A, Boissonnat J-J, Merlet J-P. On computing four-finger equilibrium and force-closure grasps of polyhedral objects. Int J Robot Res 1997;16(1):11–35.
[24] Jameson JW, Leifer LJ. Qusai-static analysis: a method for predicting grasp stability. In: Proc of IEEE Int Conf on Robotics and Automation. 1986. p. 876–83.
[25] Kerr J, Roth B. Analysis of multi-fingered hands. Int J Robot Res 1986;4(4):3–17.
[26] Bicchi A, Salisbury JK, Dario P. Augmentation of grasp robustness using intrinsic tactile sensing. In: Proc of IEEE Int Conf on Robotics and Automation. 1989. p. 302–7.
[27] Nagata K, Oosaki Y, Kakikura M, Tsukune H. Delivery by hand between human and robot based on fingertip force-torque information. In: Proc of IEEE/RSJ Int Conf on Intelligent Robots and Systems. 1998. p. 3–17.